

Search for dark matter annihilation signals from unidentified *Fermi*-LAT objects with H.E.S.S.

H. ABDALLA,¹ F. AHARONIAN,^{2,3,4} F. AIT BENKHALI,³ E.O. ANGÜNER,⁵ C. ARCARO,⁶ C. ARMAND,⁷ T. ARMSTRONG ⁸ H. ASHKAR ⁹ M. BACKES ^{1,6} V. BAGHMANYAN,¹⁰ V. BARBOSA MARTINS ¹¹ A. BARNACKA,¹² M. BARNARD,⁶ Y. BECHERINI,¹³ D. BERGE ¹¹ K. BERNLÖHR ³ B. BI,¹⁴ M. BÖTTCHER ⁶ C. BOISSON ¹⁵ J. BOLMONT ¹⁶ M. DE BONY DE LAVERGNE,⁷ M. BREUHAUS,³ R. BROSE ² F. BRUN ⁹ T. BULIK,¹⁷ T. BYLUND ¹³ F. CANGEMI,¹⁶ S. CAROFF ⁷ S. CASANOVA ^{10,3} P. CHAMBERY,¹⁸ J. CATALANO,¹⁹ T. CHAND,⁶ A. CHEN ²⁰ G. COTTER ⁸ M. CURYŁO,¹⁷ H. DALGLEISH,^{1,6} J. DAMASCENE MBARUBUCYEYE ¹¹ I.D. DAVIDS,¹ J. DAVIES ⁸ J. DEVIN,¹⁸ A. DJANNATI-ATAÏ,¹⁸ A. DMYTRIIEV,¹⁵ A. DONATH,³ V. DOROSHENKO,¹⁴ L. DREYER,⁶ L. DU PLESSIS,⁶ C. DUFFY,²¹ K. EGBERTS,²² S. EINECKE,²³ G. EMERY,¹⁶ J.-P. ERNENWEIN,⁵ K. FEIJEN,²³ S. FEGAN,²⁴ A. FIASSON,⁷ G. FICHET DE CLAIRFONTAINE ¹⁵ G. FONTAINE ²⁴ S. FUNK ¹⁹ M. FÜSSLING,¹¹ S. GABICI,¹⁸ Y.A. GALLANT,²⁵ S. GHAFOURIZADE,²⁶ G. GIAVITTO ¹¹ L. GIUNTI,^{18,9} D. GLAWION ¹⁹ J.F. GLICENSTEIN ⁹ M.-H. GRONDIN,²⁷ S. HATTINGH,⁶ M. HAUPT,¹¹ G. HERMANN,³ J.A. HINTON,³ W. HOFMANN,³ C. HOISCHEN,²² T. L. HOLCH ¹¹ M. HOLLER,²⁸ M. HÖRBE,⁸ D. HORNS,²⁹ Z. HUANG,³ D. HUBER,²⁸ M. JAMROZY ¹² D. JANKOWSKY,¹⁹ F. JANKOWSKY,²⁶ V. JOSHI ¹⁹ I. JUNG-RICHARDT,¹⁹ E. KASAI,¹ K. KATARZYŃSKI,³⁰ U. KATZ,¹⁹ D. KHANGULYAN,³¹ B. KHÉLIFI ¹⁸ S. KLEPSEK,¹¹ W. KLUŻNIAK,³² NU. KOMIN ²⁰ R. KONNO ¹¹ K. KOSACK,⁹ D. KOSTUNIN ¹¹ M. KRETER,⁶ G. KUKEC MEZEK,¹³ A. KUNDU ⁶ G. LAMANNA,⁷ S. LE STUM,⁵ A. LEMIERE,¹⁸ M. LEMOINE-GOUMARD ²⁷ J.-P. LENAIN ¹⁶ F. LEUSCHNER ¹⁴ C. LEVY,¹⁶ T. LOHSE,³³ A. LUASHVILI,¹⁵ I. LYPOVA,¹¹ J. MACKEY ² J. MAJUMDAR,¹¹ D. MALYSHEV ¹⁴ D. MALYSHEV ¹⁹ V. MARANDON ³ P. MARCHEGIANI,²⁰ A. MARCOWITH,²⁵ A. MARES,²⁷ G. MARTÍ-DEVESA ²⁸ R. MARX ^{26,3} G. MAURIN,⁷ P.J. MEINTJES,³⁴ M. MEYER,¹⁹ A. MITCHELL ³ R. MODERSKI ³² L. MOHRMANN ¹⁹ A. MONTANARI ⁹ C. MOORE,²¹ P. MORRIS ⁸ E. MOULIN ⁹ J. MULLER ²⁴ T. MURACH ¹¹ K. NAKASHIMA,¹⁹ A. NAYERHODA,¹⁰ M. DE NAUROIS,²⁴ H. NDIYAVALA,⁶ J. NIEMIEC ¹⁰ A. NOEL,¹² L. OBERHOLZER,⁶ P. O'BRIEN,²¹ S. OHM ¹¹ L. OLIVERA-NIETO ³ E. DE ONA WILHELMI,¹¹ M. OSTROWSKI ¹² M. PANTER,³ S. PANNY ²⁸ R.D. PARSONS ³³ G. PERON,³ S. PITA,¹⁸ V. POIREAU ⁷ D.A. PROKHOROV,³⁵ H. PROKOPH,¹¹ G. PÜHLHOFER,¹⁴ M. PUNCH ^{18,13} A. QUIRRENBACH,²⁶ P. REICHERZER ⁹ A. REIMER ²⁸ O. REIMER,²⁸ Q. REMY,³ M. RENAUD,²⁵ F. RIEGER,³ C. ROMOLI,³ G. ROWELL ²³ B. RUDAK ³² H. RUEDA RICARTE ⁹ E. RUIZ-VELASCO ³ V. SAHAKIAN,³⁶ S. SAILER,³ H. SALZMANN,¹⁴ D.A. SANCHEZ,⁷ A. SANTANGELO ¹⁴ M. SASAKI ¹⁹ J. SCHÄFER,¹⁹ F. SCHÜSSLER ⁹ H.M. SCHUTTE ⁶ U. SCHWANKE,³³ M. SENNIAPPAN ¹³ A.S. SEYFFERT,⁶ J. N.S. SHAPOPI ¹ K. SHININGAYAMWE,¹ R. SIMONI,³⁵ A. SINHA,¹⁸ H. SOL,¹⁵ H. SPACKMAN,⁸ A. SPECOVIVUS,¹⁹ S. SPENCER ⁸ M. SPIR-JACOB,¹⁸ L. STAWARZ,¹² R. STEENKAMP,¹ C. STEGMANN,^{22,11} S. STEINMASSL ³ C. STEPPA,²² L. SUN,³⁵ T. TAKAHASHI,³⁷ T. TANAKA,³⁷ T. TAVERNIER,⁹ A.M. TAYLOR ¹¹ R. TERRIER ¹⁸ C. THORPE MORGAN,¹⁴ J. H.E. THIENSEN,⁶ M. TLUCZYKONT,²⁹ L. TOMANKOVA,¹⁹ M. TSIROU,²⁵ M. TSUJI,³¹ R. TUFFS,³ Y. UCHIYAMA,³¹ D.J. VAN DER WALT,⁶ C. VAN ELDIK ¹⁹ C. VAN RENSBURG,¹ B. VAN SOELEN,³⁴ G. VASILEIADIS,²⁵ J. VEH,¹⁹ C. VENTER,⁶ P. VINCENT,¹⁶ A. VIANA,³⁸ J. VINK,³⁵ H.J. VÖLK ³ S.J. WAGNER ²⁶ F. WERNER,³ R. WHITE,³ A. WIERZCHOLSKA ^{10,26} YU WUN WONG,¹⁹ H. YASSIN,⁶ A. YUSAFZAI,¹⁹ M. ZACHARIAS ^{6,15} R. ZANIN,³ D. ZARGARYAN ^{2,4} A.A. ZDZIARSKI,³² A. ZECH,¹⁵ S.J. ZHU ¹¹ A. ZMIJA,¹⁹ J. ZORN,³ S. ZOUARI ¹⁸ N. ŻYWUCKA,⁶

(H.E.S.S. COLLABORATION)

- ¹*University of Namibia, Department of Physics, Private Bag 13301, Windhoek 10005, Namibia*
- ²*Dublin Institute for Advanced Studies, 31 Fitzwilliam Place, Dublin 2, Ireland*
- ³*Max-Planck-Institut für Kernphysik, P.O. Box 103980, D 69029 Heidelberg, Germany*
- ⁴*High Energy Astrophysics Laboratory, RAU, 123 Hovsep Emin St Yerevan 0051, Armenia*
- ⁵*Aix Marseille Université, CNRS/IN2P3, CPPM, Marseille, France*
- ⁶*Centre for Space Research, North-West University, Potchefstroom 2520, South Africa*
- ⁷*Laboratoire d'Annecy de Physique des Particules, Univ. Grenoble Alpes, Univ. Savoie Mont Blanc, CNRS, LAPP, 74000 Annecy, France*
- ⁸*University of Oxford, Department of Physics, Denys Wilkinson Building, Keble Road, Oxford OX1 3RH, UK*
- ⁹*IRFU, CEA, Université Paris-Saclay, F-91191 Gif-sur-Yvette, France*
- ¹⁰*Instytut Fizyki Jądrowej PAN, ul. Radzikowskiego 152, 31-342 Kraków, Poland*
- ¹¹*DESY, D-15738 Zeuthen, Germany*
- ¹²*Obserwatorium Astronomiczne, Uniwersytet Jagielloński, ul. Orła 171, 30-244 Kraków, Poland*
- ¹³*Department of Physics and Electrical Engineering, Linnaeus University, 351 95 Växjö, Sweden*
- ¹⁴*Institut für Astronomie und Astrophysik, Universität Tübingen, Sand 1, D 72076 Tübingen, Germany*
- ¹⁵*Laboratoire Univers et Théories, Observatoire de Paris, Université PSL, CNRS, Université de Paris, 92190 Meudon, France*
- ¹⁶*Sorbonne Université, Université Paris Diderot, Sorbonne Paris Cité, CNRS/IN2P3, Laboratoire de Physique Nucléaire et de Hautes Energies, LPNHE, 4 Place Jussieu, F-75252 Paris, France*
- ¹⁷*Astronomical Observatory, The University of Warsaw, Al. Ujazdowskie 4, 00-478 Warsaw, Poland*
- ¹⁸*Université de Paris, CNRS, Astroparticule et Cosmologie, F-75013 Paris, France*
- ¹⁹*Friedrich-Alexander-Universität Erlangen-Nürnberg, Erlangen Centre for Astroparticle Physics, Erwin-Rommel-Str. 1, D 91058 Erlangen, Germany*
- ²⁰*School of Physics, University of the Witwatersrand, 1 Jan Smuts Avenue, Braamfontein, Johannesburg, 2050 South Africa*
- ²¹*Department of Physics and Astronomy, The University of Leicester, University Road, Leicester, LE1 7RH, United Kingdom*
- ²²*Institut für Physik und Astronomie, Universität Potsdam, Karl-Liebknecht-Strasse 24/25, D 14476 Potsdam, Germany*
- ²³*School of Physical Sciences, University of Adelaide, Adelaide 5005, Australia*
- ²⁴*Laboratoire Leprince-Ringuet, École Polytechnique, CNRS, Institut Polytechnique de Paris, F-91128 Palaiseau, France*
- ²⁵*Laboratoire Univers et Particules de Montpellier, Université Montpellier, CNRS/IN2P3, CC 72, Place Eugène Bataillon, F-34095 Montpellier Cedex 5, France*
- ²⁶*Landessternwarte, Universität Heidelberg, Königstuhl, D 69117 Heidelberg, Germany*
- ²⁷*Université Bordeaux, CNRS/IN2P3, Centre d'Études Nucléaires de Bordeaux Gradignan, 33175 Gradignan, France*
- ²⁸*Institut für Astro- und Teilchenphysik, Leopold-Franzens-Universität Innsbruck, A-6020 Innsbruck, Austria*
- ²⁹*Universität Hamburg, Institut für Experimentalphysik, Luruper Chaussee 149, D 22761 Hamburg, Germany*
- ³⁰*Institute of Astronomy, Faculty of Physics, Astronomy and Informatics, Nicolaus Copernicus University, Grudziadzka 5, 87-100 Torun, Poland*
- ³¹*Department of Physics, Rikkyo University, 3-34-1 Nishi-Ikebukuro, Toshima-ku, Tokyo 113-0033, 171-8501, Japan*
- ³²*Nicolaus Copernicus Astronomical Center, Polish Academy of Sciences, ul. Bartycka 18, 00-716 Warsaw, Poland*
- ³³*Institut für Physik, Humboldt-Universität zu Berlin, Newtonstr. 15, D 12489 Berlin, Germany*
- ³⁴*Department of Physics, University of the Free State, PO Box 339, Bloemfontein 9300, South Africa*

³⁵*GRAPPA, Anton Pannekoek Institute for Astronomy, University of Amsterdam, Science Park 904, 1098 XH Amsterdam, The Netherlands*

³⁶*Yerevan Physics Institute, 2 Alikhanian Brothers St., 375036 Yerevan, Armenia*

³⁷*Kavli Institute for the Physics and Mathematics of the Universe (WPI), The University of Tokyo Institutes for Advanced Study (UTIAS), The University of Tokyo, 5-1-5 Kashiwa-no-Ha, Kashiwa, Chiba, 277-8583, Japan*

³⁸*Now at Instituto de Física de São Carlos, Universidade de São Paulo, Av. Trabalhador São-carlense, 400 - CEP 13566-590, São Carlos, SP, Brasil*

(Dated: June 16, 2021)

ABSTRACT

Cosmological N -body simulations show that Milky Way-sized galaxies harbor a population of unmerged dark matter subhalos. These subhalos could shine in gamma-rays and be eventually detected in gamma-ray surveys as unidentified sources. We performed a thorough selection among unidentified *Fermi*-LAT Objects (UFOs) to identify them as possible TeV-scale dark matter subhalo candidates. We search for very-high-energy ($E \gtrsim 100$ GeV) gamma-ray emissions using H.E.S.S. observations towards four selected UFOs. Since no significant very-high-energy gamma-ray emission is detected in any dataset of the four observed UFOs nor in the combined UFO dataset, strong constraints are derived on the product of the velocity-weighted annihilation cross section $\langle\sigma v\rangle$ by the J -factor for the dark matter models. The 95% C.L. observed upper limits derived from combined H.E.S.S. observations reach $\langle\sigma v\rangle J$ values of 3.7×10^{-5} and 8.1×10^{-6} $\text{GeV}^2 \text{cm}^{-2} \text{s}^{-1}$ in the W^+W^- and $\tau^+\tau^-$ channels, respectively, for a 1 TeV dark matter mass. Focusing on thermal WIMPs, the H.E.S.S. constraints restrict the J -factors to lie in the range 6.1×10^{19} - 2.0×10^{21} $\text{GeV}^2 \text{cm}^{-5}$, and the masses to lie between 0.2 and 6 TeV in the W^+W^- channel. For the $\tau^+\tau^-$ channel, the J -factors lie in the range 7.0×10^{19} - 7.1×10^{20} $\text{GeV}^2 \text{cm}^{-5}$ and the masses lie between 0.2 and 0.5 TeV. Assuming model-dependent predictions from cosmological N -body simulations on the J -factor distribution for Milky Way-sized galaxies, the dark matter models with masses greater than 0.3 TeV for the UFO emissions can be ruled out at high confidence level.

Keywords: Dark matter, High energy astrophysics, Gamma-ray sources, Gamma-ray telescopes

1. INTRODUCTION

The presence of dark matter (DM) is suggested by a wealth of astrophysical and cosmological measurements, however its underlying nature is yet unknown. Among the most promising candidates are weakly interacting massive particles (WIMPs): particles thermally-produced in the early universe with mass and coupling strength at the electroweak scale predict a present relic density (Steigman et al. 2012) consistent with that observed today (Adam et al. 2016). WIMP self-annihilation would produce Standard Model particles including gamma rays which for a long time, have been recognized as a prime messenger to indirectly detect DM annihilation or decay. Gamma rays are not deflected by magnetic fields and therefore point back to their sources. Among the most promising DM targets observed by ground-based imaging atmospheric Cherenkov telescopes (IACTs) such as H.E.S.S. are

the Galactic Centre (Abdallah et al. 2016, 2018) and nearby dwarf galaxies (Aharonian et al. 2008a; Abramowski et al. 2011, 2014; Abdalla et al. 2018).

Other compelling and complementary DM targets for IACTs are DM subhalos populating galactic halo (see, e.g., Kamionkowski et al. 2010). The observed universe today is believed to have formed hierarchically with the smallest structures first. DM particles first collapse into gravitationally-bound systems that later merge to form the first subhalos, which subsequently form more massive ones. The merging history leads to DM halos massive enough to retain gas and trigger star formation and give rise to the galaxies we observe today. However, most of the subhalos remain completely dark. Assuming that DM is made of WIMPs, they could shine in gamma rays. The annihilation process in subhalos could be frequent enough to be detectable by IACTs provided that the WIMPs are sufficiently massive. If DM subhalos are made of WIMPs, 10^{-4} to 10^{10} M_{\odot} mass subhalos are expected to lie in DM halos of Milky Way-sized galaxies (Diemand et al. 2008; Springel et al. 2008b), with the most massive of them ($\gtrsim 10^8 M_{\odot}$) hosting dwarf galaxies.

DM subhalos are predicted to be compact and concentrated, and are not expected to harbour conventional astrophysical high-energy emitters. Provided they are close and/or massive enough, DM annihilations in these objects could produce gamma-ray fluxes detectable with satellite and ground-based experiments such as IACTs (Calcaneo-Roldan & Moore 2000; Tasitsiomi & Olinto 2002; Stoehr et al. 2003; Koushiappas et al. 2004). However, their actual location in the galaxy is not known. Their search can be performed using all-sky gamma-ray observations (see, for instance, Diemand et al. 2007) such as with the Large Area Telescope (LAT) instrument onboard the Fermi satellite (see, for instance, Berlin & Hooper 2014) or wide-field surveys carried out with IACTs (see, for instance, Aharonian et al. 2008b; Brun et al. 2011).

All-sky *Fermi*-LAT observations revealed a population of sources that lack associated signals from observations at other wavelengths (Ajello et al. 2017; Abdollahi et al. 2020). These sources are therefore classified as unidentified Fermi objects (UFOs). If the DM particle mass lies below 100 GeV, some UFOs detected by *Fermi*-LAT could be potentially described by DM models (Belikov et al. 2012; Zechlin et al. 2012; Bertoni et al. 2015, 2016; Calore et al. 2017; Coronado-Blazquez et al. 2019) Identifying some of the UFOs as DM subhalos require however higher ($\gtrsim 100$ GeV) DM masses given their hard gamma-ray spectra in the few-ten-to-hundred GeV energy range. Such objects are therefore excellent targets for IACTs to perform searches for TeV DM subhalos. In 2018 and 2019, the H.E.S.S. collaboration carried out an observational campaign for a selection of the most promising UFOs in order to probe their potential TeV-mass DM-induced emission.

The paper is organized as follows. Section 2 presents the expected DM-induced gamma-ray signals from Galactic subhalos. Section 3 describes the selection procedure of UFOs as DM subhalo candidates relevant for H.E.S.S. observations along with the *Fermi*-LAT data analysis of the selected UFOs as DM subhalo candidates. In Sec. 4, the H.E.S.S. observations and data analysis of the selected UFOs are presented. The constraints from H.E.S.S. observations on DM-induced emission models for the UFOs are derived in Sec. 5. Section 6 and Sec. 7 are devoted to the discussion of the results obtained in this work and to a general summary, respectively.

2. DARK MATTER ANNIHILATION SIGNALS

2.1. *Expected gamma-ray flux from dark matter annihilation*

The energy-differential gamma-ray flux expected from the self-annihilation of Majorana DM particles of mass m_{DM} can be expressed as

$$\frac{d\Phi_\gamma(E_\gamma, \Delta\Omega)}{dE_\gamma} = \frac{\langle\sigma v\rangle}{8\pi m_{\text{DM}}^2} \sum_f \text{BR}_f \frac{dN^f}{dE_\gamma} J(\Delta\Omega), \quad \text{with} \quad J(\Delta\Omega) = \int_{\Delta\Omega} \int_{\text{los}} \rho^2(s(r, \theta)) ds d\Omega. \quad (1)$$

$\langle\sigma v\rangle$ is the thermally-averaged velocity-weighted annihilation cross section, and $\sum_f \text{BR}_f dN^f/dE_\gamma$ is the sum of the annihilation spectra dN^f/dE_γ per annihilation in the final states f with associated branching ratios BR_f . The expected DM annihilation signal consists of a continuum spectrum of gamma rays extending up to the DM mass, and possibly a line-like feature close to the DM mass. The former contribution arises from the hadronization and/or decay of quarks, heavy leptons, and gauge bosons involved in the annihilation process. The latter comes from the direct annihilation into γX with $X = \gamma, h, Z$ or a non-Standard Model neutral particle, providing a spectral line at an energy $E_\gamma = m_{\text{DM}}[1 - (m_X/2m_{\text{DM}})^2]$. When the DM particles self-annihilate into charged particles, gamma rays are produced via processes involving virtual internal bremsstrahlung and final state radiation. These processes provide an additional bump-like feature that peaks at an energy close to the DM mass.

The term $J(\Delta\Omega)$, hereafter referred to the J -factor, corresponds to the integration of the square of the DM density over the line-of-sight (los) s and solid angle $\Delta\Omega$. As opposed to objects with measured stellar dynamics like dwarf galaxies, UFOs have unknown distances to Earth and their J -factors cannot be derived from stellar kinematics.

2.2. Expected subhalo J -factor distribution in the Milky Way

Cosmological N -body simulations (see, for instance, Refs. (Diemand et al. 2008; Springel et al. 2008b)) predict Milky Way (MW)-sized galaxy halos to harbor today unmerged DM substructures called galactic subhalos. These simulations make robust predictions on the slope and normalization of the subhalo mass function defined as $d \ln N/d \ln M \propto M^{-\alpha_m}$, with a slope $\alpha_m \simeq 1.9$ for MW-like galaxies (see, for instance, Refs. (Diemand et al. 2008; Springel et al. 2008a; Gao et al. 2012; Fiacconi et al. 2017)). Galactic subhalos are not expected to host conventional high-energy astrophysical sources and a large number density of subhalos in MW-like galaxies with high DM concentrations is expected. Only closeby and massive enough subhalos are expected to provide detectable gamma-ray signals.

The cosmological simulations provide the abundance of the resolved subhalos, their radial distribution and structural properties such as their mass and concentration, and suggest a DM distribution in the subhalos following a cuspy density profile, that can be well described by NFW (Navarro et al. 1997) or Einasto (Springel et al. 2008c) parametrizations. The limited spatial resolution of the current simulations can only probe the slope of the radial DM density distribution in a subhalo for the most massive subhalos. Assuming a parametrization of the DM density distribution in subhalos, the distribution of J -factors of the galactic subhalo population, dN/dJ , can be derived. The cumulative J -factor distribution, $N(J) \equiv N(\geq J)$, is defined as number of subhalos with a J -factor higher than or equal to specified.

In order to derive the J -factor distribution of DM subhalos in the MW, the CLUMPY code v3.0.0 (Charbonnier et al. 2012; Bonnavard et al. 2016; Hütten et al. 2019a) is used. 1000 simulations of a MW-like galaxy are performed with a smooth NFW (Navarro et al. 1997) DM main

halo profile with the parameters corresponding to the best-fit NFW parameters presented in a recent study of DM distribution in the Milky Way (Cautun et al. 2020). For each simulation, the subhalo parameters were chosen similar to the ones used in Ref. (Hütten et al. 2016) for the “HIGH” model. The power-law slope of the subhalo mass function is chosen to be $\alpha_m = 1.9$ (Diemand et al. 2008); the number of objects between 10^8 and $10^{10}M_\odot$ is taken as $N_{\text{calib}} = 300$ following Springel et al. (2008b); and the subhalo mass-concentration relation following the distance-dependent prescription of Moliné et al. (2017). From each simulation the Galactic coordinates of all subhalos and their J -factors integrated in circular regions with 0.1° radius around the centres of gravity of the subhalos are derived.

The cumulative J -factor distribution $N(\geq J)$ is shown in the upper panel of Fig. 1 for subhalos located at Galactic latitudes $|b| > 5^\circ$. The solid red curve shows the averaged distribution computed from all the realizations and the shaded region shows the formal 1σ statistical dispersion calculated over all simulated MW-like galaxies. In the lower panel of Fig. 1, the red-dashed curve illustrates the probability to find in any simulation at least one subhalo with a J -factor higher than specified. The blue-dotted curve corresponds to the probability to find three or more subhalos. The horizontal black-dashed line gives the 5% probability: the probability on average to find one or more subhalos

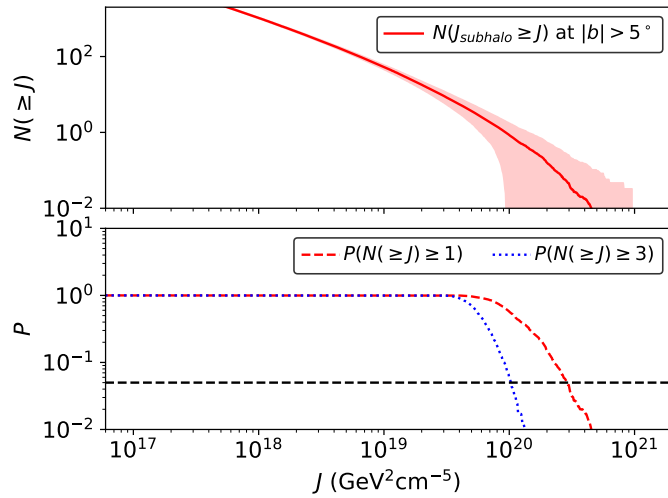


Figure 1. *Top panel:* Cumulative J -factor distribution, $N(\geq J)$, of a Milky Way-like subhalo population. The number of subhalos with a J -factor exceeding a given value is plotted (red solid curve). The red-shaded band corresponds to the 1σ statistical uncertainty obtained from 1000 simulations of the subhalo population for MW-like galaxies. *Bottom panel:* Probability P to find at least one subhalo with a J -factor higher than specified (red dashed line). The blue dotted line presents the same probability for at least three subhalos. The horizontal black dashed line shows the 5% probability. See text for more details.

with J -factor $J \geq 3 \times 10^{20} \text{ GeV}^2\text{cm}^{-5}$ (three or more subhalos with J -factors $J \geq 1 \times 10^{20} \text{ GeV}^2\text{cm}^{-5}$) is only about 5%.

3. *Fermi*-LAT UNIDENTIFIED SOURCES AS DARK MATTER SUBHALO CANDIDATES

A hypothetical gamma-ray emission from a DM subhalo would show-up in the all-sky gamma-ray surveys (Kamionkowski et al. 2010) as unidentified objects, *i.e.*, detected with the Fermi satellite but

without counterparts at any other wavelengths. A smoking-gun signature for DM detection is a very distinct energy cut-off close to the DM particle mass, assuming the two-body annihilation process taking place almost at rest. For sufficiently-large DM particle masses, *i.e.*, above a few hundred GeV, the energy cut-off could be too high in energy to be measurable by the LAT instrument onboard the Fermi satellite within a reasonable observation time. The combination of *Fermi*-LAT and IACT observations is therefore mandatory for DM subhalo searches with unidentified sources detected by the *Fermi*-LAT.

3.1. Selection procedure for H.E.S.S. observations

In order to determine the best candidates for H.E.S.S. observations among the unidentified *Fermi*-LAT sources, a thorough selection has been performed in the Third Catalog of High-Energy *Fermi*-LAT Sources (3FHL) (Ajello et al. 2017) which comprises pointlike sources detected above 10 GeV. The source selection requires the unidentified sources to be steady, *i.e.*, to not show flux variability over time according to 3FHL catalogue¹, exhibiting a hard power-law spectral index ($\Gamma < 2$), as expected for DM-induced signals for DM masses above 100 GeV with no obvious conventional counterpart at other wavelengths. The multi-wavelength (MWL) search for possible counterparts is based on the Fermi-LAT source coordinates : for each source, counterparts are searched in catalogs of MWL facilities (*XMM-Newton*, *ROSAT*, *SUZAKU*, *CGRO*, *Chandra*, *Swift*, *WMAP*, *RXTE*, *Nustar*, *SDSS*, *Planck*, *WISE*, *HST*) assuming a searched radius around the source determined by the position uncertainty derived in the 3FHL catalogue. The unidentified *Fermi*-LAT sources are usually quite faint and only the ones sufficiently far away from the Galactic plane are considered in order to avoid challenging background modelling connected to Galactic plane diffuse emission in the *Fermi*-LAT energy range. The selected sources do not lie in a complex astrophysical environment, *i.e.*, they are relatively isolated with no high-energy gamma-ray emission within about one degree². In addition, a maximum zenith angle of 45° for H.E.S.S. observations is required in order to obtain low energy thresholds. The selection criteria were applied on the 3FHL source catalog and are summarized in Tab. 1. The small number of suitable DM subhalo candidates obtained by a straightforward selection confirms that the observation of a selection of UFOs is a viable DM search strategy for targeted observations performed by IACTs. Only four UFOs were eventually observed due to H.E.S.S. observational program scheduling constraints. The characteristics of the UFOs selected for observations with the H.E.S.S. telescopes are summarized in Tab. 2.

¹ While the criterium on the variability provides steady candidates as expected for DM sources, *Fermi*-LAT photon properties at the highest energies have been checked. None of them could be attributed to flaring of nearby *Fermi*-LAT sources.

² The closest 3FHL source for 3FHL J1915.2-1323 is at 0.8° while for the other UFOs, the closest source is at distance higher than 1.7° .

Criteria	Numbers of sources
Without association	178
Far enough from the Galactic plane, cut in Galactic latitude of $ b > 5^\circ$	126
Non-variable, cut in variability index (No. of Bayesian blocks in var. analysis) equal to 1	125
Maximum zenith angle at H.E.S.S. site of 45°	83
Follow a simple power law with significance for curvature $< 3\sigma$	83
Hard spectrum, cut in spectral index below 2	18
No MWL counterparts	6

Table 1. Criteria applied to 3FHL catalog for the selection of DM subhalo candidates. For the multi-wavelength (MWL) counterpart search, individual search radii were used ($\sim 2 - 4$ arcmin) based on the uncertainty of the Fermi position quoted in the 3FHL. The following list of MWL facilities was checked: *XMM-Newton*, *ROSAT*, *SUZAKU*, *CGRO*, *Chandra*, *Swift*, *WMAP*, *RXTE*, *Nustar*, *SDSS*, *Planck*, *WISE*, *HST*.

Name	RA	Dec.	TS for $E \geq 10$ GeV	Position uncertainty [arcmin]	Pivot energy [GeV]	Spectral energy distribution at pivot energy [10^{-13} TeV cm $^{-2}$ s $^{-1}$]	Power-law index	$\Delta\chi^2$	E_{cut} [GeV]
	[degrees]	[degrees]							
3FHL J0929.2-4110	142.3345	-41.1833	36	2.4	0.39	0.12 ± 0.01	1.37 ± 0.07	0.15	> 33
3FHL J1915.2-1323 [†]	288.8182	-13.3916	23	3.0	62.8	2.1 ± 0.9	1.5 ± 0.4	0.05	> 35
3FHL J2030.2-5037	307.5901	-50.6344	40	2.6	6.3	1.9 ± 0.3	1.85 ± 0.1	0.40	> 67
3FHL J2104.5+2117 ^{a,b}	316.1226	21.2831	58	2.2	1.56	5.3 ± 0.5	2.22 ± 0.06	0.02	> 85

^a The spectral index in the 3FHL catalogue is 1.8 (Ajello et al. 2017).

^b 3FHL J2104.5.2117 was recently associated in the 4FGL catalogue (Abdollahi et al. 2020) with an AGN with a probability of 0.4.

Table 2. Properties of the selected UFOs together with their spectral parameters. The second and third columns provides the RA-Dec coordinates of the UFOs along with their test statistics (TS) values for energies above 10 GeV in the fourth column. The fifth column gives their position uncertainty. Pivot energy, spectral energy distribution at the pivot energy and best-fit power-law spectral index are given in the sixth, seventh, eighth columns, respectively. The ninth column provides the $\Delta\chi^2$ value between a pure power-law and a power law with exponential cut-off fit to the data. The last column gives the 95% C.L. lower limit on a possible energy cut-off in the energy spectrum. The 3FHL J1915.2-1323 source marked with [†] is detected only above 10 GeV. For this source the spectral index, pivot energy, differential flux and $\Delta\chi^2$ value are given for this energy band. For the other sources these quantities are given for energies higher than 0.1 GeV.

3.2. Fermi-LAT data analysis on the selected objects

Fermi-LAT data selected for the analysis presented in this paper were collected over a time span of more than 12 years (Aug. 2008 to Oct. 2020). The latest available `fermitools` v. 2.0.0 with P8R3_V3 response functions (CLEAN photon class)³ are used. The initial stage of the analysis aims at determining the energy spectra of UFO sources. In order to extract the differential energy spectrum for each object the standard binned likelihood analysis of a 14° -radius region around each of the considered objects is performed for a set of eight log-equal energy bins in the range 0.1 – 1000 GeV. The spectral analysis is based on the fitting of a spatial and spectral model of the sky region around the source of interest to the data. The model of the region includes: (*i*): all sources from the most recent

³ See description of *Fermi*-LAT response functions.

4FGL-DR2 catalogue (Abdollahi et al. 2020) within the 14° -radius region around UFO position; (ii): components for isotropic and Galactic diffuse emissions given by the standard spatial and spectral templates `iso_P8R3_CLEAN_V2_v1.txt` and `gll_iem_v07.fits`, respectively. For the fitting procedure the spectral models of these sources are selected according to the 4FGL catalogue with all parameters except normalisation fixed to the catalogue values. In addition 4FGL sources up to 10° beyond the considered region of interest are included in the model, with all their parameters fixed to the catalogue values in order to reduce the bias connected to a possible presence of bright sources outside the considered region and effects connected to the poor PSF of the LAT at low (~ 0.1 GeV) energies. The UFO spectra are modelled by a pure power-law function with the slope defined from a broad energy-range fit. Following the recommendation of the *Fermi*-LAT collaboration, our analysis is performed with energy dispersion handling enabled. We additionally checked that the test-statistic maps of the considered regions do not show significant residuals between the data and the model, see Appendix A for more details. We conclude that the considered models well describe the UFO sources' regions.

Table 2 summarizes the analysis results for each UFO. Given the available photon statistics in the *Fermi*-LAT dataset of the selected objects, a power-law spectrum with a (super)-exponential energy cut-off in the TeV energy range, as expected from DM-induced emissions (Belikov & Silk 2013), and a pure power-law emission cannot be significantly discriminated, see Tab. 2 for a corresponding change $\Delta\chi^2$ between these models. The last column of Tab. 2 summarises 95% C.L. *Fermi*-LAT lower limits on the energy cutoff, defined as the energy at which $\Delta\chi^2$ changes by 2.71 between power-law and exponential energy cut-off power-law models.

3.3. Dark matter models for the selected sources

Figure 2 shows DM annihilation models together with *Fermi*-LAT flux measurements. Model predictions for DM masses of 1 TeV and 10 TeV, respectively, are plotted separately for the W^+W^- and $\tau^+\tau^-$ annihilation channels. Some DM models are able to qualitatively describe the observed gamma-ray flux from the selected UFOs. For instance, the predictions shown for $m_{\text{DM}} = 1$ TeV describe well the *Fermi*-LAT data for 3FHL J0929.2-4110 in the W^+W^- and $\tau^+\tau^-$ annihilation channels. Instead, For 3FHL J2030.2-5037, the predictions for $m_{\text{DM}} = 1$ TeV in the $\tau^+\tau^-$ annihilation channel provide a poor description of the emission while a better one is obtained in the W^+W^- one.

In order to assess quantitatively the above statements on viable DM-induced emission models, the spectrum of each UFO is explicitly modelled with a DM-annihilation induced spectral template⁴. For given m_{DM} and annihilation channel, the model is characterised only by the overall normalisation of the spectra given by $\langle\sigma v\rangle J$. To identify the range of viable parameters for DM annihilation, a scan over a large range of $\langle\sigma v\rangle J$ is performed.

A test-statistic (TS) is defined as a difference between best-fit log-likelihood functions for models with no DM emission (\mathcal{L}_0 , “background only” hypothesis) and the model (\mathcal{L}) which includes the UFO source described by the corresponding parameter $\langle\sigma v\rangle J$: $TS = -2\log(\mathcal{L}/\mathcal{L}_0)$ (Mattox et al. 1996)⁵. Negative TS values correspond to the detection of the source, *i.e.*, adding a source with a corresponding parameter *improves* the fit in comparison to background-only hypothesis.

⁴ Provided within `fermitools` as `DMFitFunction` based on Ref. (Jeltema & Profumo 2008)

⁵ The TS value for a source with N -parametric (spectral) model follows a χ^2 distribution with N degrees of freedom in the high statistic limit (Wilks 1938).

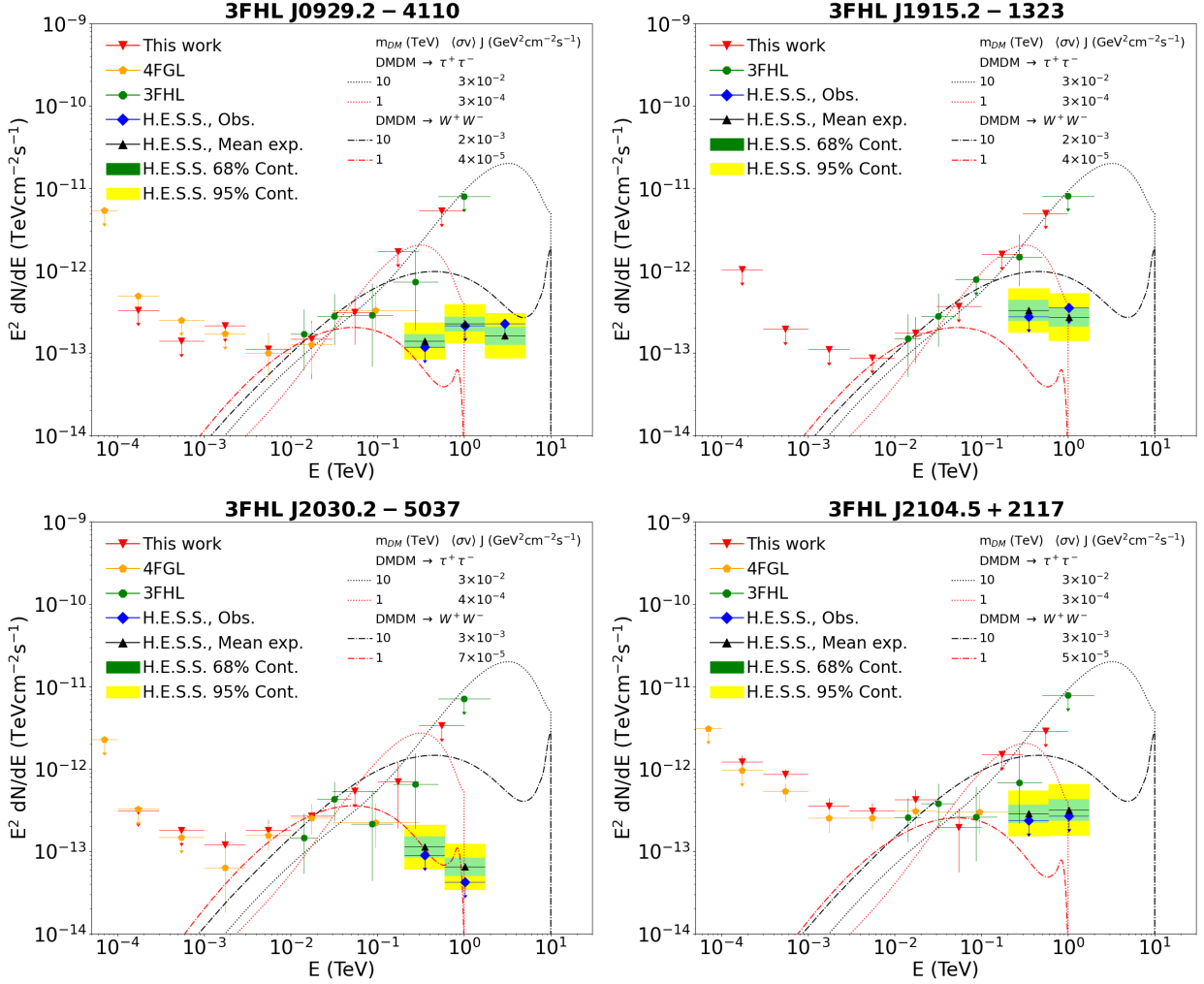


Figure 2. Spectral energy distributions of the selected unidentified Fermi objects observed with *Fermi*-LAT and H.E.S.S. for 3FHL J0929.2-4110 (top left), 3FHL J1915.2-1323 (top right), 3FHL J2030.2-5037 (bottom left), and 3FHL J2104.5+2117 (bottom right), respectively. The differential flux points computed in this work from the *Fermi*-LAT dataset (red dots) and taken from the 4FGL (orange dots) and from the 3FHL (green dots) catalogues (Ajello et al. 2017; Abdollahi et al. 2020), are shown with the vertical and horizontal error bars corresponding to the 1σ statistical errors and the bin size, respectively. Upper limit points (red, orange and green arrows) are given at 95% C.L.. The observed flux upper limits from H.E.S.S. observations (blue arrows) are plotted at 95% C.L., together with the mean expected flux upper limits (black) and the 1σ (green) and 2σ (yellow) containment bands. Overlaid are theoretical DM-induced fluxes for 1 TeV and 10 TeV DM masses in the W^+W^- (dash-dotted lines) and $\tau^+\tau^-$ (dotted lines) annihilation channels, respectively.

The left panels of Fig. 3 illustrate the results for a single UFO 3FHL J0929.2-4110 for W^+W^- (top) and $\tau^+\tau^-$ (bottom) annihilation channels, respectively. For each $\langle\sigma v\rangle J$, the color scale shows TS values. Assuming that the TS follows a χ^2 distribution, a TS equal to -9 , (resp. -25) would correspond to a 3σ (resp. 5σ) detection for 1 degree of freedom. The dashed cyan and orange lines shows the detection region that corresponds to the improvement of TS by -9 and -25 , respectively. The right panels in Fig. 3 present the results for the analysis of the combined datasets of the three

selected UFOs (3FHL J0929.2-4110 ; 3FHL J1915.2-1323; 3FHL J2030.2-5037) obtained through the combination of the log-likelihood profiles from individual objects, for W^+W^- (top) and $\tau^+\tau^-$ (bottom) annihilation channels, respectively.

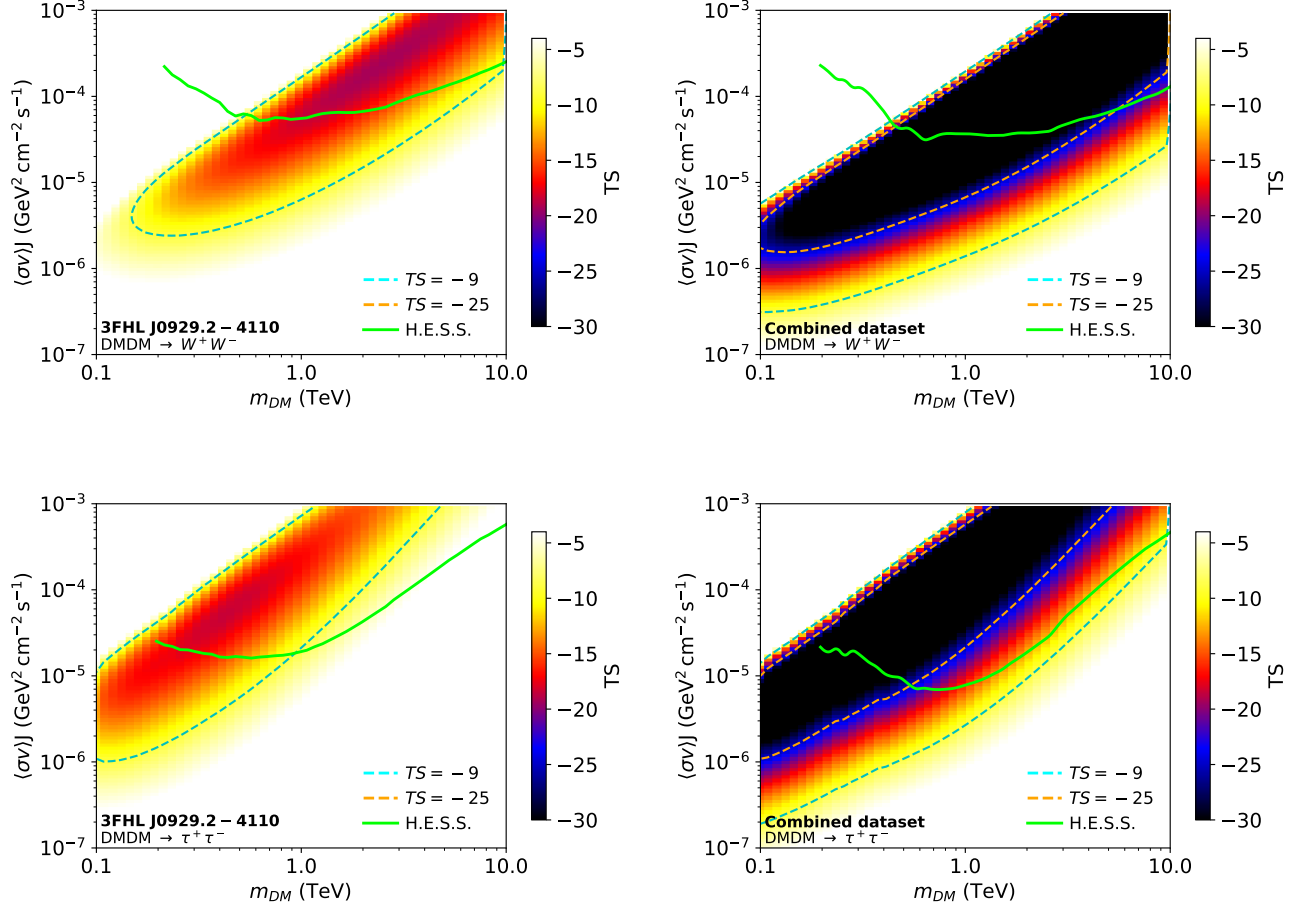


Figure 3. Contours of TS computed from *Fermi*-LAT datasets on the 3FHL J0929.2-4110 (left panels) and the combined UFO datasets (right panels), respectively. The contours are given in the $(\langle\sigma v\rangle J, m_{DM})$ plane for the W^+W^- (upper panels) and $\tau^+\tau^-$ (lower panels) annihilation channel. The cyan and orange dashed lines show the -9 and -25 TS contours. Overlaid (solid green line) are H.E.S.S. upper limits displayed at 95% C.L. Contours of TS for 3FHL J1915.2-1323, 3FHL J2030.2-5037 and 3FHL J2104.5+2117 are shown in Fig. 7 in Appendix.

4. H.E.S.S. OBSERVATIONS AND ANALYSIS

4.1. Data analysis

H.E.S.S. is an array of five IACTs located in the Khomas Highland in Namibia, at an altitude of 1800 m. The array is composed of four 12 m diameter telescopes (CT1-4) and a fifth 28 m diameter telescope (CT5) at the middle of the array. The observations presented here were performed in 2018 and 2019 with the full five-telescope array for the selection of unidentified Fermi-LAT objects presented in Tab. 2. They were carried out in the *wobble* mode, where the telescope pointing direction

is offset from the nominal target position by an angle between 0.5° and 0.7° . The observations for the data analysis are selected according to the standard run selection criteria (Aharonian et al. 2006). After the calibration of raw shower images recorded in the camera, the reconstruction of the direction and energy of the gamma-ray events is performed in a template-fitting technique (de Naurois & Rolland 2009) in which the recorded images are compared to pre-calculated showers computed from a semi-analytical model. An energy resolution of 10% and an angular resolution of 0.06° at 68% containment radius for gamma-ray energies above 200 GeV are achieved. The results described here have been cross-checked with an independent calibration and analysis chain yielding compatible results (Parsons & Hinton 2014).

The selected UFOs are assumed to be pointlike sources according to the point spread function (PSF) of *Fermi*-LAT which reaches $\sim 0.1^\circ$ above 100 GeV. Given the H.E.S.S. PSF, the region of interest (ROI), hereafter referred to as the ON source region, is therefore defined as for pointlike-emission searches for H.E.S.S. and the ROI is taken as a disk of 0.12° radius. The residual background is measured in OFF regions according to the *MultipleOff* technique (Aharonian et al. 2006). For each telescope pointing position, the OFF regions are defined at the same distance from the pointing position as for the ON region, which leads to identical acceptances in the ON and OFF regions. An excluded region defined as a disk of radius equal to twice the ON-region radius is used in order to avoid any leakage of the searched signal into the OFF regions. The α parameter is defined as the ratio between the solid angle size of the OFF and ON regions by $\alpha = \Delta\Omega_{\text{OFF}}/\Delta\Omega_{\text{ON}}$. The excess significance in the ROI is computed following the statistical approach of Ref. (Li & Ma 1983). Table 3 summarizes for each UFO the live time, the mean zenith angle of the observations, the ON and OFF counts, the α parameter averaged over all the observations, as well as the excess significance in the ROI. No significant gamma-ray excess is found, neither in the ON source region, nor anywhere else in the field of view.

Name	Live time [hours]	Mean zenith angle [degrees]	N_{ON} [counts]	N_{OFF} [counts]	$\bar{\alpha}$	Significance [σ]
3FHL J0929.2-4110	27.4	29.0	424	5884	13.9	0.1
3FHL J1915.2-1323	3.6	19.4	87	1181	13.9	0.2
3FHL J2030.2-5037	9.8	31.3	160	2192	13.9	0.1
3FHL J2104.5+2117	6.8	46.7	73	853	13.9	1.1

Table 3. H.E.S.S. data analysis results for each UFO. The second and third columns give the live time and mean zenith angle of the H.E.S.S. observations, respectively. Count numbers measured in the ON and OFF regions are given in the fourth and fifth columns, respectively, with the α parameter averaged over all observations, $\bar{\alpha}$, given in the sixth column. The seventh column provides the measured excess significance between the ON and OFF counts.

Since no significant excess is found from any of the selected UFOs, energy-differential observed flux upper limits are computed at 95% C.L. assuming the best-fit power-law spectral index derived from the *Fermi*-LAT data analysis. Expectations for the energy-differential flux upper limits are computed from 100 independent Poisson realizations of the measured OFF counts for the ON and OFF regions. From the realizations, mean and standard deviation values are extracted and used to compute the 68% and 95% containment bands. The differential flux upper limits are shown in Fig. 2 with an energy binning of 0.5 dex. The expectations and the containment bands for the upper limits shown

in the figure are computed including 25% systematic uncertainty. Assuming a power-law spectral index of 2 would change the differential flux upper limits by less than 6%.

4.2. Upper limit computation for the DM emission

A binned Poisson maximum likelihood analysis is performed to search for spectral features expected from DM annihilation signals with respect to the background. For each UFO, the H.E.S.S. energy range is divided into 62 logarithmically-spaced bins from 100 GeV up to 70 TeV. For a given DM mass and annihilation channel, the Poisson likelihood function in the energy bin i can be written as

$$\mathcal{L}_i(N_i^S, N_i^B | N_{\text{ON}}, N_{\text{OFF}}, \alpha) = \frac{(N_i^S + N_i^B)^{N_{\text{ON},i}}}{N_{\text{ON},i}!} e^{-(N_i^S + N_i^B)} \frac{(N_i^{S'} + \alpha N_i^B)^{N_{\text{OFF},i}}}{N_{\text{OFF},i}!} e^{-(N_i^{S'} + \alpha N_i^B)}. \quad (2)$$

$N_{\text{ON},i}$ and $N_{\text{OFF},i}$ stand for the number of measured events in the ON and OFF regions, respectively. N_i^B is the expected number of background events in the ON region. N_i^S and $N_i^{S'}$ are the expected number of DM signal events in the ON and OFF regions, respectively. They are computed by folding the expected theoretical DM flux given in Eq. (1) with the energy-dependent acceptance and energy resolution of H.E.S.S. for the considered data set. The term dN/dE_γ^f in Eq. (1) is extracted from Ref. (Cirelli et al. 2011) for each assumed DM mass and annihilation channel. The energy resolution of H.E.S.S. is represented by a Gaussian function with a width of $\sigma_E/E = 10\%$ above 200 GeV. The UFOs are also pointlike sources for H.E.S.S., therefore no leakage is expected in the background region and $N_i^{S'}$ is taken to $N_i^{S'} \equiv 0$. The likelihood function for a given object \mathcal{L} is defined as $\mathcal{L} = \prod_i \mathcal{L}_i$.

Since no significant excess is found in any of the selected UFOs by H.E.S.S., upper limits can be derived assuming UFOs are DM-induced gamma-ray emitters from a likelihood ratio test statistic (TS) given by:

$$TS = -2 \log \frac{\mathcal{L}(N^S(\langle\sigma v\rangle J), \widehat{N}^B(\langle\sigma v\rangle J) | N_{\text{ON}}, N_{\text{OFF}}, \alpha)}{\mathcal{L}(\widehat{N}^S(\langle\sigma v\rangle J), \widehat{N}^B | N_{\text{ON}}, N_{\text{OFF}}, \alpha)}. \quad (3)$$

\widehat{N}_i^B is obtained through a conditional maximization, achieved by solving $d\mathcal{L}/dN_i^B = 0$. \widehat{N}_i^S and \widehat{N}_i^B are computed using an unconditional maximization. Following the procedure defined in Ref. (Cowan et al. 2011), upper limits are computed assuming a positive signal, *i.e.*, $\widehat{N}_i^S > 0$. The $\langle\sigma v\rangle J$ value for which the TS value is equal to 2.71 provides the one-sided 95% confidence level (C.L.) upper limit on the quantity $\langle\sigma v\rangle J$.

The hypothesis that all UFOs are indeed DM subhalos, but too faint to be detected as such in the TeV energy range with the given exposure, can be tested when the individual datasets are combined. If no significant overall excess is found in the combined dataset, combined upper limits on $\langle\sigma v\rangle J$ can be derived versus the DM mass assuming J to be an averaged J -factor. In Eq. (3), the likelihood function is replaced by the combined likelihood expressed as $\mathcal{L}_{\text{comb}} = \prod_{j=1}^{N_{\text{targets}}} \mathcal{L}_j$, where \mathcal{L}_j is the likelihood of the target j .

5. RESULTS

No significant excess is measured in any of the H.E.S.S. datasets of the selected UFOs. 95% C.L. upper limits on $\langle\sigma v\rangle J$ are derived versus the DM mass using Eq. (3). Figure 4 shows for each UFO the upper limits as a function of the DM mass for the W^+W^- and $\tau^+\tau^-$ annihilation channels,

respectively. In most of the DM mass range, the strongest constraints are reached for 3FHL J0929.2-4110 observations. For a 1 TeV DM mass, the constraints $\langle\sigma v\rangle J = 5.5\times 10^{-5} \text{ GeV}^2\text{cm}^{-2}\text{s}^{-1}$ and $1.9\times 10^{-5} \text{ GeV}^2\text{cm}^{-2}\text{s}^{-1}$ in W^+W^- and $\tau^+\tau^-$ annihilation channels, respectively, for 3FHL J0929.2-4110.

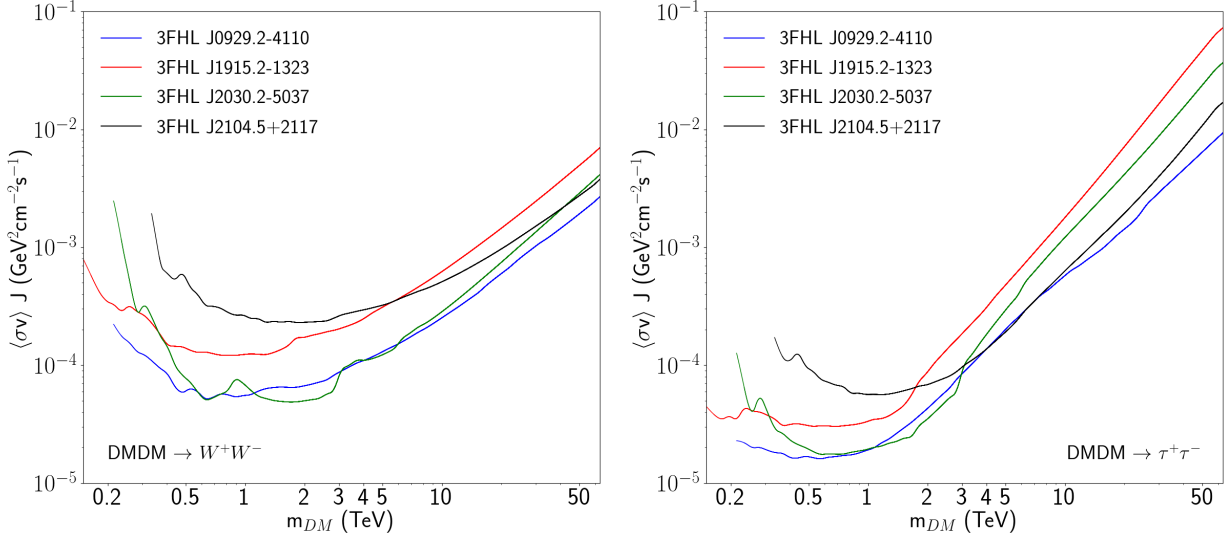


Figure 4. 95% C.L. upper limits on the product of the annihilation cross section $\langle\sigma v\rangle$ and the J -factor J as a function of the DM mass m_{DM} in the W^+W^- (left panel) and $\tau^+\tau^-$ (right panel) annihilation channels for 3FHL J0929.2-4110 (blue line), 3FHL J1915.2-1323 (red line), 3FHL J2030.2-5037 (green line), and 3FHL J2104.5+2117 (black line), respectively.

The combined analysis of the four H.E.S.S. datasets does not show any significant excess. Therefore, the UFO datasets are combined and upper limits on $\langle\sigma v\rangle J$ are computed. Given its possible association with an AGN, the source 3FHL J2104.5+2117 is removed to provide conservative combined upper limits. The right panel of Fig. 3 shows the combined 95% C.L. upper limits on $\langle\sigma v\rangle J$ as a function of the DM mass for the W^+W^- and $\tau^+\tau^-$ annihilation channels, respectively. The analysis of the combined datasets allows for an improvement of about 10% and 20% for 1 TeV DM mass in the W^+W^- and $\tau^+\tau^-$ annihilation channel, respectively, with respect to the most constraining upper limit from the individual UFO datasets. The combined limits reach 3.7×10^{-5} and $8.1\times 10^{-6} \text{ GeV}^2\text{cm}^{-2}\text{s}^{-1}$ in the W^+W^- and $\tau^+\tau^-$ channels, respectively, for a 1 TeV DM mass.

In order to derive the J -factor values required to explain the UFO emission in terms of DM models, the value of the annihilation cross section expected for thermal WIMPs ($\langle\sigma v\rangle_{\text{th}} \simeq 3\times 10^{-26} \text{ cm}^3\text{s}^{-1}$) is used (Steigman et al. 2012). The J -factor upper limits for the DM models of the UFOs as function of the DM mass are given at 95% C.L. in Fig. 5. For a 1 TeV DM mass in the W^+W^- channel, the J -factor values are constrained to be between 2.4×10^{20} and $1.3\times 10^{21} \text{ GeV}^2\text{cm}^{-5}$ for DM models with $TS \leq -25$ (which corresponds to $\geq 5\sigma$ confidence interval assuming TS follows χ^2 distribution). For a DM mass of 10 TeV in the W^+W^- channel, all the J -factor values for DM models with $TS \leq -25$ are ruled out at 95% C.L. by the H.E.S.S. constraints. In the $\tau^+\tau^-$ channels, the H.E.S.S. constraints are even stronger. For 300 GeV DM mass, the allowed J -factor values are between 1.4×10^{20} and

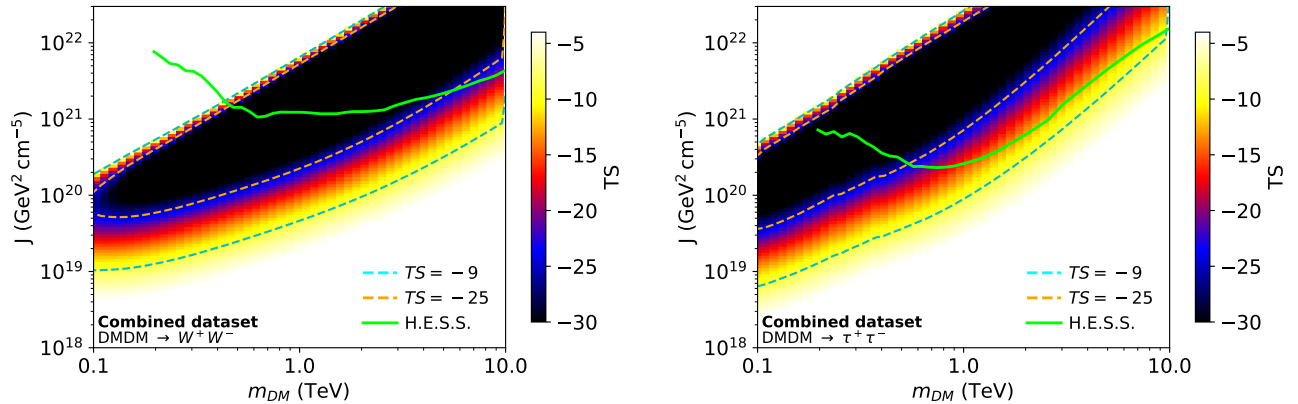


Figure 5. Contours of TS computed from the *Fermi*-LAT combined UFO datasets. The contours are given in the (J, m_{DM}) plane for the W^+W^- (left panel) and $\tau^+\tau^-$ (right panel) annihilation channel, assuming the $\langle\sigma v\rangle$ value expected for thermal WIMPs. The cyan and orange dashed lines show the -9 and -25 TS contours. Overlaid (solid green line) are the H.E.S.S. 95% C.L. upper limits from the combined UFO datasets.

$5.9 \times 10^{20} \text{ GeV}^2 \text{cm}^{-5}$ for $TS \leq -25$ DM models. The H.E.S.S. upper limits restrict the J -factors to lie in the range $6.1 \times 10^{19} - 2.0 \times 10^{21} \text{ GeV}^2 \text{cm}^{-5}$ and the masses to lie between 0.2 and 6 TeV in the W^+W^- channel. For the $\tau^+\tau^-$ channel, the J -factors lie in the range $7.0 \times 10^{19} - 7.1 \times 10^{20} \text{ GeV}^2 \text{cm}^{-5}$ and the masses lie between 0.2 and 0.5 TeV.

Using predictions of N-body cosmological simulations, the number of subhalos with a J -factor higher than a given value for a MW-like galaxy can be extracted as displayed in Fig. 1. The probability to have at least three subhalos with a J -factor higher than $10^{20} \text{ GeV}^2 \text{cm}^{-5}$ is below 5% (Fig. 1, blue-dotted line). According to this prediction, the interpretation of the UFO emissions in terms of DM particle annihilations in Galactic DM subhalos can be further constrained from Fig. 5 to $m_{\text{DM}} \lesssim 1 \text{ TeV}$ for W^+W^- and $m_{\text{DM}} \lesssim 0.3 \text{ TeV}$ for $\tau^+\tau^-$ channels.

6. DISCUSSION

A substantial number of UFOs may emit gamma rays from DM annihilations in subhalos. However, some of them could be active galactic nuclei or other types of galaxies that lack so far detection at other wavelengths. Alternative astrophysical interpretations of UFOs as pulsars or low-luminosity globular clusters hosting millisecond pulsars (Mirabal et al. 2016), may be less plausible since typical gamma-ray spectra for these types of objects are characterised by an energy cut-off at energies of a few GeV.

The cumulative J -factor distribution is in very good agreement with the results of Hütten et al. (2016) for the "HIGH" model intended to predict the highest possible number of subhalos in a typical MW-like galaxy. The real number of DM subhalos can be an order of magnitude smaller as shown for the predictions in the "LOW" model of Hütten et al. (2016). The choice of the number of subhalos of masses between 10^8 and $10^{10} M_{\odot}$ of $N_{\text{calib}} = 300$ is motivated by the output of DM-only simulations Springel et al. (2008b). Baryon feedback can significantly reduce this value, up to a factor of two (Mollitor et al. 2015; Sawala et al. 2016). This would make the highest J -factor values even more unlikely. As discussed in Coronado-Blázquez et al. (2019), subhalos with the highest J -factors

should appear as extended sources for *Fermi*-LAT given its point spread function of about 0.1° above 10 GeV. However, even these brightest DM subhalos would produce faint gamma-ray sources whose spatial extension would be challenging to measure for *Fermi*-LAT. On the simulation front, further work is likely needed to use predictions for subhalo angular sizes in MW-like galaxies to definitely rule out pointlike UFOs as potential DM subhalos.

The DM density distribution of the Galactic halo is assumed here to follow a NFW parametrization. Incorporating hydrodynamics and baryon feedback in cosmological simulations tend to soften the inner cusp of the DM profiles in Milky Way-like galaxies, leading to a flattening of order 1 kpc (see, for instance, [Chan et al. 2015](#)). However, these predictions for the expected DM distribution have large uncertainties due to the effects of baryonic physics. The resolution limit of the simulations at sufficiently small distances becomes also pertinent. Alternative Galactic mass models can be used to describe subhalo parameters for Milky Way-like galaxies ([Catena & Ullio 2010](#); [McMillan 2011](#); [Stref & Lavalle 2017](#); [McMillan 2017](#)). Using different Galactic mass models, the subhalo luminosity functions derived in [Stref & Lavalle \(2017\)](#) provide compatible results. Considering a core profile would make the high DM mass exclusion of the DM models for the UFO emission even stronger. DM subhalos could also have cored profiles with lower DM concentration, which would make them more prone to tidal disruption. This would therefore decrease both the normalisation of the J -factor distribution function and shift it to lower values. The J -factor distribution prediction is based on DM-only Via Lactea-II simulations using WMAP cosmology. The simulations based on the most recent cosmological results from the Planck mission with added baryonic physics could somewhat change the predicted properties of the MW subhalos. The effect of baryon feedback and tidal effects induced by both DM and baryons is likely to alter the DM concentration of subhalos ([Despali & Vegetti 2017](#); [Stref & Lavalle 2017](#)). Details of the modeling of tidal disruption of Galactic DM subhalos on the brightest subhalo can be found in [Di Mauro et al. \(2020\)](#). Therefore, the cumulative J -factor distribution would be shifted to lower values. In this case, the DM-induced interpretation of the UFO emission would be even more constrained given that the probability to find high J -factor values would be even smaller. The presence of baryons affects both the amplitude and the slope of the DM halo and subhalo mass functions. It can reduce the slope by a few percent in the $10^6 - 10^9 M_\odot$ subhalo mass range ([Benson 2020](#)), which can also alter the rate of subhalos with large J factors. No cut is applied to the maximal value of the subhalo mass when computing the cumulative J -factor distribution. While subhalos with masses of about $10^7 M_\odot$ or higher may be able to host star formation and actually be dwarf galaxies, simulations including hydrodynamics and feedback physics in addition to the gravitational effects for the expected DM distribution in both the main halo and its subhalos such as in [Zhu et al. \(2016\)](#), show that a significant fraction of subhalos with masses of about $10^9 M_\odot$ is found to host no stars. For subhalo masses larger than 10^7 - $10^8 M_\odot$, a noticeable fraction of them can start triggering star formation and indeed form a faint dwarf galaxy. Arguably these masses critically depend on the baryonic physics implementation in the simulations and its associated feedback. Considering subhalos with masses lower than $10^7 M_\odot$ implies the probability to have at least one subhalo with $J \geq 3 \times 10^{20} \text{ GeV}^2 \text{ cm}^{-5}$ to be about 0.3%, therefore a factor of about 16 lower than in the case without mass cut.

The interpretation of UFOs as DM subhalos of TeV-mass scale thermal WIMPs requires J -factors in excess of a few $10^{20} \text{ GeV}^2 \text{ cm}^{-5}$. Such J -factor values are only occasionally obtained in N-body simulations of MW-type galaxies. The highest subhalo J -factor values are usually subject to a large

statistical variance. The precise value of the brightest subhalos can be subject to a large uncertainty, implying a factor-of-ten uncertainty on the J -factor value for $J \gtrsim 10^{20} \text{ GeV}^2\text{cm}^{-5}$ in the "HIGH" model (Hütten et al. 2019b)⁶. Previous studies using *Fermi*-LAT data only searched for UFOs as promising DM subhalo candidates for DM masses below 100 GeV (see, for instance, Bertoni et al. 2015, 2016; Coronado-Blázquez et al. 2019). For instance, in the study of Coronado-Blázquez et al. (2019), masses of few ten GeV are ruled out for canonical thermal WIMPs. The present analysis searches for UFOs as DM subhalos for the uncharted TeV-mass thermal WIMP models.

The maximal value of subhalo J -factors obtained in simulations is model dependent and can be increased even in comparison to the optimistic estimate of the J -factor distribution considered here as discussed below. The normalisation of the subhalo mass function assumes usually about 10% of the total DM halo content to be in the form of subhalos, with the total DM halo density being normalized to the DM density at the location of the Sun $\rho(r_\odot) = \rho_\odot = 0.39 \text{ GeVcm}^{-3}$. The precise value is subject to uncertainties of a factor of 1.5 to 2 (Read 2014). Varying the input parameters of the simulations in the relevant ranges of interest, such as $\rho_\odot = 0.6 \text{ GeVcm}^{-3}$ and the scale radius of the main DM halo $r_s = 25 \text{ kpc}$, would increase the highest J -factor values by a factor of two. The predicted cumulative J -factor distribution would therefore probe higher J -factor values. Considering substructures in galactic subhalos (see, for instance, Hiroshima et al. (2018)) results in higher expected J -factor values for the Galactic subhalo population with typical increase factors of a few, therefore shifting the cumulative J -factor distribution to higher values.

The above-mentioned large systematic uncertainties in the prediction of the J -factor distribution weaken significantly the constraints from cosmological simulations, which makes them comparable to or weaker than the H.E.S.S. constraints in, *e.g.*, the $\tau^+\tau^-$ channel. This makes the model-independent H.E.S.S. constraints the only relevant ones for robust interpretation of UFOs as Galactic subhalos of annihilating DM.

7. SUMMARY

In this work, a straightforward filtering of the unidentified sources in the 3FHL point-source catalogue has been performed using selection cuts to identify the most promising DM subhalo candidates for DM masses above a few hundred GeV. The datasets for the four UFOs were collected with the Fermi satellite in a 12-year observation period. Using H.E.S.S. observations, no significant signal has been detected from any of the selected UFOs. From H.E.S.S. flux upper limits, DM models describing the UFO emissions with high significance are strongly constrained in the TeV DM mass range for different annihilation channels. Assuming thermally-produced DM particles, the DM models for the UFO emissions require high J -factor values. When the model-dependent predictions from N -body simulations of the MW-like subhalo population are taken into account, the required high J -factor values for the DM models explaining the UFOs as Galactic subhalos are unlikely. This can point towards interpretation of the UFOs as subhalos of relatively light WIMPs with masses $m_{\text{DM}} \lesssim 0.3 \text{ TeV}$ for which somewhat lower J -factors are preferred. However, this could be in tension with constraints on thermal WIMPs from dwarf galaxy observations by *Fermi*-LAT (Ackermann et al. 2015; Albert et al. 2017).

⁶ Using the "LOW" model for the predictions of the J -factor distribution would make the interpretation of UFOs as DM subhalos even more unlikely given that the probability to get high J -factor values would be lowered compared to what it would be in the "HIGH" model.

ACKNOWLEDGEMENTS

The support of the Namibian authorities and of the University of Namibia in facilitating the construction and operation of H.E.S.S. is gratefully acknowledged, as is the support by the German Ministry for Education and Research (BMBF), the Max Planck Society, the German Research Foundation (DFG), the Helmholtz Association, the Alexander von Humboldt Foundation, the French Ministry of Higher Education, Research and Innovation, the Centre National de la Recherche Scientifique (CNRS/IN2P3 and CNRS/INSU), the Commissariat à l'énergie atomique et aux énergies alternatives (CEA), the U.K. Science and Technology Facilities Council (STFC), the Knut and Alice Wallenberg Foundation, the National Science Centre, Poland grant no. 2016/22/M/ST9/00382, the South African Department of Science and Technology and National Research Foundation, the University of Namibia, the National Commission on Research, Science & Technology of Namibia (NCRST), the Austrian Federal Ministry of Education, Science and Research and the Austrian Science Fund (FWF), the Australian Research Council (ARC), the Japan Society for the Promotion of Science and by the University of Amsterdam.

We appreciate the excellent work of the technical support staff in Berlin, Zeuthen, Heidelberg, Palaiseau, Paris, Saclay, Tübingen and in Namibia in the construction and operation of the equipment. This work benefitted from services provided by the H.E.S.S. Virtual Organisation, supported by the national resource providers of the EGI Federation.

REFERENCES

- Abdalla, H., et al. 2018, *JCAP*, 11, 037, doi: [10.1088/1475-7516/2018/11/037](https://doi.org/10.1088/1475-7516/2018/11/037)
- Abdallah, H., et al. 2016, *Phys. Rev. Lett.*, 117, 111301, doi: [10.1103/PhysRevLett.117.111301](https://doi.org/10.1103/PhysRevLett.117.111301)
- . 2018, *Phys. Rev. Lett.*, 120, 201101, doi: [10.1103/PhysRevLett.120.201101](https://doi.org/10.1103/PhysRevLett.120.201101)
- Abdollahi, S., et al. 2020, *Astrophys. J. Suppl.*, 247, 33, doi: [10.3847/1538-4365/ab6bcb](https://doi.org/10.3847/1538-4365/ab6bcb)
- Abramowski, A., et al. 2011, *Astropart. Phys.*, 34, 608, doi: [10.1016/j.astropartphys.2010.12.006](https://doi.org/10.1016/j.astropartphys.2010.12.006)
- . 2014, *Phys. Rev.*, D90, 112012, doi: [10.1103/PhysRevD.90.112012](https://doi.org/10.1103/PhysRevD.90.112012)
- Ackermann, M., et al. 2015, *Phys. Rev. Lett.*, 115, 231301, doi: [10.1103/PhysRevLett.115.231301](https://doi.org/10.1103/PhysRevLett.115.231301)
- Adam, R., et al. 2016, *Astron. Astrophys.*, 594, A1, doi: [10.1051/0004-6361/201527101](https://doi.org/10.1051/0004-6361/201527101)
- Aharonian, F., et al. 2006, *Astron. Astrophys.*, 457, 899, doi: [10.1051/0004-6361:20065351](https://doi.org/10.1051/0004-6361:20065351)
- . 2008a, *Astropart. Phys.*, 29, 55, doi: [10.1016/j.astropartphys.2007.11.007](https://doi.org/10.1016/j.astropartphys.2007.11.007)
- . 2008b, *Phys. Rev. D*, 78, 072008, doi: [10.1103/PhysRevD.78.072008](https://doi.org/10.1103/PhysRevD.78.072008)
- Ajello, M., et al. 2017, *Astrophys. J. Suppl.*, 232, 18, doi: [10.3847/1538-4365/aa8221](https://doi.org/10.3847/1538-4365/aa8221)
- Albert, A., et al. 2017, *Astrophys. J.*, 834, 110, doi: [10.3847/1538-4357/834/2/110](https://doi.org/10.3847/1538-4357/834/2/110)
- Belikov, A. V., Hooper, D., & Buckley, M. R. 2012, *Phys. Rev. D*, 86, 043504, doi: [10.1103/PhysRevD.86.043504](https://doi.org/10.1103/PhysRevD.86.043504)
- Belikov, A. V., & Silk, J. 2013, *Phys. Rev. Lett.*, 111, 071302, doi: [10.1103/PhysRevLett.111.071302](https://doi.org/10.1103/PhysRevLett.111.071302)
- Benson, A. J. 2020, *Mon. Not. Roy. Astron. Soc.*, 493, 1268, doi: [10.1093/mnras/staa341](https://doi.org/10.1093/mnras/staa341)
- Berlin, A., & Hooper, D. 2014, *Phys. Rev. D*, 89, 016014, doi: [10.1103/PhysRevD.89.016014](https://doi.org/10.1103/PhysRevD.89.016014)
- Bertoni, B., Hooper, D., & Linden, T. 2015, *JCAP*, 12, 035, doi: [10.1088/1475-7516/2015/12/035](https://doi.org/10.1088/1475-7516/2015/12/035)
- . 2016, *JCAP*, 05, 049, doi: [10.1088/1475-7516/2016/05/049](https://doi.org/10.1088/1475-7516/2016/05/049)
- Bonnivard, V., Hütten, M., Nezri, E., et al. 2016, *Computer Physics Communications*, 200, 336, doi: [10.1016/j.cpc.2015.11.012](https://doi.org/10.1016/j.cpc.2015.11.012)
- Brun, P., Moulin, E., Diemand, J., & Glicenstein, J.-F. 2011, *Phys. Rev. D*, 83, 015003, doi: [10.1103/PhysRevD.83.015003](https://doi.org/10.1103/PhysRevD.83.015003)
- Calcaneo-Roldan, C., & Moore, B. 2000, *Phys. Rev. D*, 62, 123005, doi: [10.1103/PhysRevD.62.123005](https://doi.org/10.1103/PhysRevD.62.123005)
- Calore, F., De Romeri, V., Di Mauro, M., Donato, F., & Marinacci, F. 2017, *Phys. Rev. D*, 96, 063009, doi: [10.1103/PhysRevD.96.063009](https://doi.org/10.1103/PhysRevD.96.063009)
- Catena, R., & Ullio, P. 2010, *JCAP*, 08, 004, doi: [10.1088/1475-7516/2010/08/004](https://doi.org/10.1088/1475-7516/2010/08/004)
- Cautun, M., Benítez-Llambay, A., Deason, A. J., et al. 2020, *MNRAS*, 494, 4291, doi: [10.1093/mnras/staa1017](https://doi.org/10.1093/mnras/staa1017)
- Chan, T. K., Kereš, D., Oñorbe, J., et al. 2015, *Mon. Not. Roy. Astron. Soc.*, 454, 2981, doi: [10.1093/mnras/stv2165](https://doi.org/10.1093/mnras/stv2165)
- Charbonnier, A., Combet, C., & Maurin, D. 2012, *Computer Physics Communications*, 183, 656, doi: [10.1016/j.cpc.2011.10.017](https://doi.org/10.1016/j.cpc.2011.10.017)
- Cirelli, M., et al. 2011, *JCAP*, 1103, 051, doi: [10.1088/1475-7516/2012/10/E01](https://doi.org/10.1088/1475-7516/2012/10/E01), [10.1088/1475-7516/2011/03/051](https://doi.org/10.1088/1475-7516/2011/03/051)
- Coronado-Blazquez, J., Sanchez-Conde, M. A., Dominguez, A., et al. 2019, *JCAP*, 07, 020, doi: [10.1088/1475-7516/2019/07/020](https://doi.org/10.1088/1475-7516/2019/07/020)
- Coronado-Blázquez, J., Sánchez-Conde, M. A., Di Mauro, M., et al. 2019, doi: [10.1088/1475-7516/2019/11/045](https://doi.org/10.1088/1475-7516/2019/11/045)
- Cowan, G., Cranmer, K., Gross, E., & Vitells, O. 2011, *European Physical Journal C*, 71, 1554, doi: [10.1140/epjc/s10052-011-1554-0](https://doi.org/10.1140/epjc/s10052-011-1554-0)
- de Naurois, M., & Rolland, L. 2009, *Astropart. Phys.*, 32, 231, doi: [10.1016/j.astropartphys.2009.09.001](https://doi.org/10.1016/j.astropartphys.2009.09.001)
- Despali, G., & Vegetti, S. 2017, *Mon. Not. Roy. Astron. Soc.*, 469, 1997, doi: [10.1093/mnras/stx966](https://doi.org/10.1093/mnras/stx966)
- Di Mauro, M., Stref, M., & Calore, F. 2020, *Phys. Rev. D*, 102, 103010, doi: [10.1103/PhysRevD.102.103010](https://doi.org/10.1103/PhysRevD.102.103010)
- Diemand, J., Kuhlen, M., & Madau, P. 2007, *Astrophys. J.*, 657, 262, doi: [10.1086/510736](https://doi.org/10.1086/510736)
- Diemand, J., Kuhlen, M., Madau, P., et al. 2008, *Nature*, 454, 735, doi: [10.1038/nature07153](https://doi.org/10.1038/nature07153)
- Fiacconi, D., Mayer, L., Madau, P., et al. 2017, *Mon. Not. Roy. Astron. Soc.*, 467, 4080, doi: [10.1093/mnras/stx335](https://doi.org/10.1093/mnras/stx335)
- Gao, L., Navarro, J., Frenk, C., et al. 2012, *Mon. Not. Roy. Astron. Soc.*, 425, 2169, doi: [10.1111/j.1365-2966.2012.21564.x](https://doi.org/10.1111/j.1365-2966.2012.21564.x)

- Hiroshima, N., Ando, S., & Ishiyama, T. 2018, *Phys. Rev. D*, 97, 123002, doi: [10.1103/PhysRevD.97.123002](https://doi.org/10.1103/PhysRevD.97.123002)
- Hütten, M., Combet, C., Maier, G., & Maurin, D. 2016, *J. Cosmology Astropart. Phys.*, 2016, 047, doi: [10.1088/1475-7516/2016/09/047](https://doi.org/10.1088/1475-7516/2016/09/047)
- Hütten, M., Combet, C., & Maurin, D. 2019a, *Computer Physics Communications*, 235, 336, doi: [10.1016/j.cpc.2018.10.001](https://doi.org/10.1016/j.cpc.2018.10.001)
- Hütten, M., Stref, M., Combet, C., Lavalle, J., & Maurin, D. 2019b, *Galaxies*, 7, 60, doi: [10.3390/galaxies7020060](https://doi.org/10.3390/galaxies7020060)
- Jeltema, T. E., & Profumo, S. 2008, *J. Cosmology Astropart. Phys.*, 2008, 003, doi: [10.1088/1475-7516/2008/11/003](https://doi.org/10.1088/1475-7516/2008/11/003)
- Kamionkowski, M., Koushiappas, S. M., & Kuhlen, M. 2010, *Phys. Rev. D*, 81, 043532, doi: [10.1103/PhysRevD.81.043532](https://doi.org/10.1103/PhysRevD.81.043532)
- Koushiappas, S. M., Zentner, A. R., & Walker, T. P. 2004, *Phys. Rev. D*, 69, 043501, doi: [10.1103/PhysRevD.69.043501](https://doi.org/10.1103/PhysRevD.69.043501)
- Li, T. P., & Ma, Y. Q. 1983, *ApJ*, 272, 317, doi: [10.1086/161295](https://doi.org/10.1086/161295)
- Mattox, J. R., Bertsch, D. L., Chiang, J., et al. 1996, *ApJ*, 461, 396, doi: [10.1086/177068](https://doi.org/10.1086/177068)
- McMillan, P. J. 2011, *MNRAS*, 414, 2446, doi: [10.1111/j.1365-2966.2011.18564.x](https://doi.org/10.1111/j.1365-2966.2011.18564.x)
- . 2017, *MNRAS*, 465, 76, doi: [10.1093/mnras/stw2759](https://doi.org/10.1093/mnras/stw2759)
- Mirabal, N., Charles, E., Ferrara, E., et al. 2016, *Astrophys. J.*, 825, 69, doi: [10.3847/0004-637X/825/1/69](https://doi.org/10.3847/0004-637X/825/1/69)
- Moliné, Á., Sánchez-Conde, M. A., Palomares-Ruiz, S., & Prada, F. 2017, *MNRAS*, 466, 4974, doi: [10.1093/mnras/stx026](https://doi.org/10.1093/mnras/stx026)
- Mollitor, P., Nezri, E., & Teyssier, R. 2015, *Mon. Not. Roy. Astron. Soc.*, 447, 1353, doi: [10.1093/mnras/stu2466](https://doi.org/10.1093/mnras/stu2466)
- Navarro, J. F., Frenk, C. S., & White, S. D. M. 1997, *Astrophys. J.*, 490, 493, doi: [10.1086/304888](https://doi.org/10.1086/304888)
- Parsons, R. D., & Hinton, J. A. 2014, *Astropart. Phys.*, 56, 26, doi: [10.1016/j.astropartphys.2014.03.002](https://doi.org/10.1016/j.astropartphys.2014.03.002)
- Read, J. 2014, *J. Phys. G*, 41, 063101, doi: [10.1088/0954-3899/41/6/063101](https://doi.org/10.1088/0954-3899/41/6/063101)
- Sawala, T., et al. 2016, *Mon. Not. Roy. Astron. Soc.*, 457, 1931, doi: [10.1093/mnras/stw145](https://doi.org/10.1093/mnras/stw145)
- Springel, V., White, S. D. M., Frenk, C. S., et al. 2008a, *Nature*, 456, 73, <https://arxiv.org/abs/0809.0894>
- Springel, V., Wang, J., Vogelsberger, M., et al. 2008b, *Mon. Not. Roy. Astron. Soc.*, 391, 1685, doi: [10.1111/j.1365-2966.2008.14066.x](https://doi.org/10.1111/j.1365-2966.2008.14066.x)
- Springel, V., White, S. D. M., Frenk, C. S., et al. 2008c, *Nature*, 456, 73
- Steigman, G., Dasgupta, B., & Beacom, J. F. 2012, *Phys. Rev.*, D86, 023506, doi: [10.1103/PhysRevD.86.023506](https://doi.org/10.1103/PhysRevD.86.023506)
- Stoehr, F., White, S. D. M., Springel, V., Tormen, G., & Yoshida, N. 2003, *Mon. Not. Roy. Astron. Soc.*, 345, 1313, doi: [10.1046/j.1365-2966.2003.07052.x](https://doi.org/10.1046/j.1365-2966.2003.07052.x)
- Stref, M., & Lavalle, J. 2017, *Phys. Rev. D*, 95, 063003, doi: [10.1103/PhysRevD.95.063003](https://doi.org/10.1103/PhysRevD.95.063003)
- Tasitsiomi, A., & Olinto, A. V. 2002, *Phys. Rev. D*, 66, 083006, doi: [10.1103/PhysRevD.66.083006](https://doi.org/10.1103/PhysRevD.66.083006)
- Wilks, S. S. 1938, *The Annals of Mathematical Statistics*, 9, 60, <http://www.jstor.org/stable/2957648>
- Zechlin, H. S., Fernandes, M. V., Elsaesser, D., & Horns, D. 2012, *Astron. Astrophys.*, 538, A93, doi: [10.1051/0004-6361/201117655](https://doi.org/10.1051/0004-6361/201117655)
- Zhu, Q., Marinacci, F., Maji, M., et al. 2016, *Mon. Not. Roy. Astron. Soc.*, 458, 1559, doi: [10.1093/mnras/stw374](https://doi.org/10.1093/mnras/stw374)

APPENDIX

A. TEST-STATISTIC MAPS FOR THE UFO SOURCES FROM FERMI-LAT DATASETS

In this section we present the results for the search of possible sources not accounted by the considered model based on 4FGL catalogue of the UFOs vicinity. We built test-statistics (TS) maps for $5^\circ \times 5^\circ$ region centered at the position of each UFO. These maps illustrate the significance ($\sim \sqrt{TS}$) above the background model of a test point-like source with a power-law spectrum characterised by a free normalisation and slope fixed to -2, in each pixel.

For the background model, where the corresponding UFO source is removed, we consider the same spatial/spectral models as used for the analysis of *Fermi*-LAT data described in Sec. 3.2. Such a choice of the background model allows us to check the presence of unaccounted sources close to UFOs' positions as well as verify the point-like spatial morphology of the emission associated with the UFO.

Fig. 6 show the TS maps for all four UFO sources for energies above 10 GeV in Galactic coordinates with pixel size of 0.05° . No smoothing is applied to the maps. Cyan crosses show the positions of UFO sources. Green circles indicate the position of the nearby 4FGL sources included in the background model. The maps indicate the absence of significant residuals which could affect the *Fermi*-LAT analysis of the UFOs.

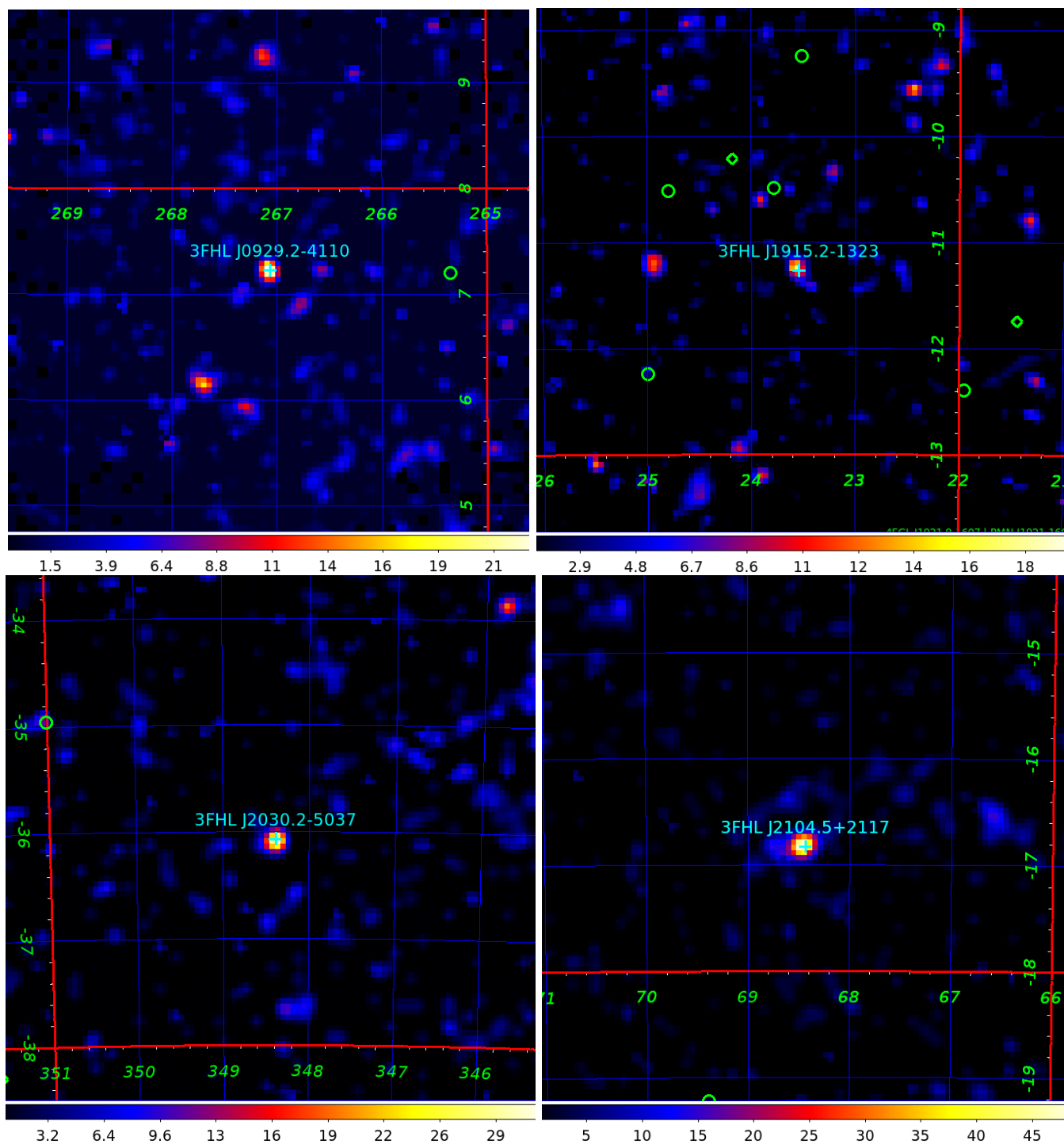


Figure 6. Test statistics maps for $5^\circ \times 5^\circ$ region around each of the considered UFOs for energies above 10 GeV in Galactic coordinates with pixel size of 0.05° . The color scale indicates the values of the TS. No smoothing to the map is applied. Cyan crosses show the position of corresponding UFO source. Green crosses show positions of nearby 4FGL sources included in the background model.

B. CONTOURS OF TS FROM FERMI-LAT DATASETS ON THE 3FHL J1915.2-1323, 3FHL J2030.2-5037, 3FHL J2104.5+2117 FOR THE W^+W^- AND $\tau^+\tau^-$ ANNIHILATION CHANNELS, RESPECTIVELY.

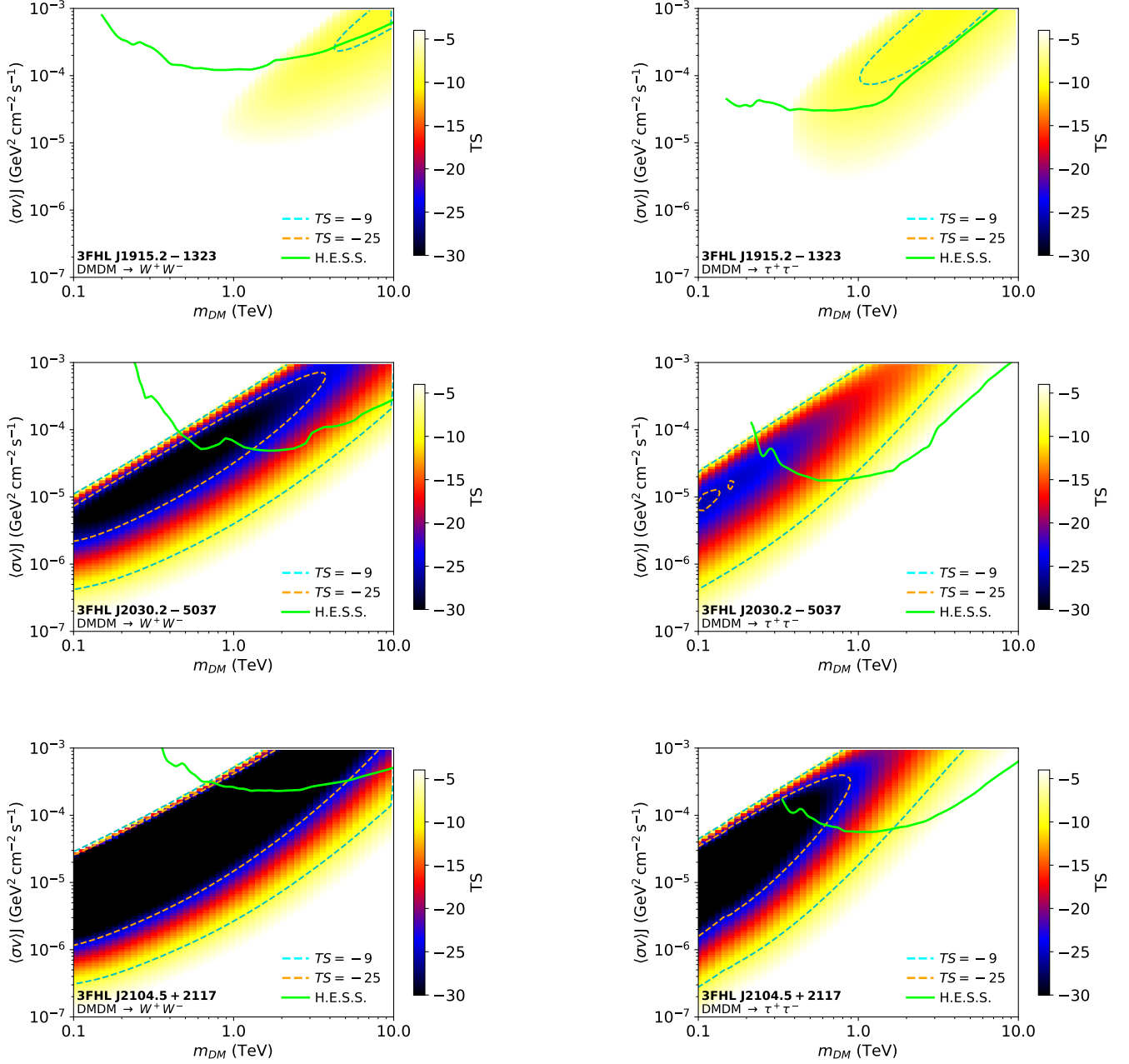


Figure 7. Contours of TS computed from *Fermi*-LAT datasets on 3FHL J1915.2-1323 (upper panels), 3FHL J2030.2-5037 (middle panels), 3FHL J2104.5+2117 (lower panels), respectively. The contours are given in the $(\langle\sigma v\rangle J, m_{DM})$ plane for the W^+W^- (left panels) and $\tau^+\tau^-$ (right panels) annihilation channel. The cyan and orange dashed lines show the -9 and -25 TS contours. Overlaid (solid green line) are the H.E.S.S. constraints displayed at 95% C.L.